PCCP

Accepted Manuscript

ROYAL SOCIETY OF CHEMISTRY

www.rsc.org/pccp

Journal Name

RSCPublishing

ARTICLE

Construction of flexible photoelectrochemical solar cells based on ordered nanostructural BiOI/Bi_2S_3 heterojunction films

Cite this: DOI: 10.1039/x0xx00000x

Received 00th January 2012,
Accepted 00th January 2012

DOI: 10.1039/x0xx00000x

www.rsc.org/

Mingqing Fang,[ab] Huimin Jia,[a] Weiwei He, [a] Yan Lei,[a] Lizhi Zhang*[b] and Zhi Zheng*[a]

Ordered 2D nanostructual BiOI nanoflake arrays decorated with Bi_2S_3 nanospheres have been designed and *in-situ* fabricated for the first time, to form BiOI/Bi_2S_3 bulkheterojunctions through a soft chemical route. A modified successive ionic layer adsorption and reaction (SILAR) method was developed to fabricate BiOI nanoflake arrays on flexible ITO/PET substrates at room temperature. The degree of transformation of BiOI to Bi_2S_3 was controlled through the adjustment of exposure time of BiOI/ITO substrate to thioacetamide (TAA) aqueous solution. The morphologies of BiOI, BiOI/Bi_2S_3 heterojunctions and Bi_2S_3 films were examined by scanning electron microscopy (SEM), X-ray powder diffraction (XRD) patterns, and high resolution transmission electron microscopy (HRTEM). The presence of Bi_2S_3 was further validated through Raman spectra and X-ray photoelectron spectra (XPS). Especially, photoelectrochemical measurements demonstrated that such Bi_2S_3 decorated BiOI photoanode based cell exhibits significant augments of short-circuit current density (J_{sc}) and incident photon-to-current conversion efficiency (IPCE, 3 times higher than pure BiOI photoanode), attributable to the stronger photo absorption and better photogenerated charge carrier separation and transport efficiency. The surface photovoltage (SPV) measurements further confirmed the importance of BiOI/Bi_2S_3 heterojunctions in such PEC cells. This solution-based process directly on flexible ITO offers the promise for low-cost, large-area, roll-to-roll application of the manufacturing of the third generation thin-film photovoltaic devices.

1. Introduction

The utilization of solar energy is one applicable solution to meet the rapidly increasing energy demands world-wide. Among all the photovoltaics, ZnO and TiO_2 based solar cells have progressed tremendously in the past decades[1-3] since the first report of dye-sensitized solar cell.[4] However, ZnO and TiO_2 are both poor candidates due to their low absorption from the solar spectrum. Therefore, it is essential to develop new narrow gap semiconductors to exploit the solar energy.

BiOI, a p-type semiconductor with band gap of approximately 1.8 eV,[5-7] has been extensively studied due to its unique optical properties, such as infrared absorption spectrum,[8] Raman spectrum,[9] fluorescence spectrum[10] and reflection spectrum.[11] The band structure and energy level have also been investigated.[10, 12] Due to an appropriate band gap, low cost and environmentally friendly nature, BiOI has been widely used as efficient photocatalyst to degrade various kinds of organic pollutant[13-19] and as an electrochemical hydrogen storage material.[7] To develop a stronger photo-response and more efficient charge carrier separation, materials scientists have developed different BiOI-based heterojunctions.[20-23] However, the photoelectrochemical properties of BiOI films are rarely studied.[5, 17] Furthermore, most BiOI and BiOI-based materials are prepared by solvothermal method at relatively high temperatures,[24] which consumes energy.

The successive ionic layer adsorption and reaction (SILAR) method[25] is a solution processing application that has been utilized extensively to deposit a film at room temperature and has numerous advantages such as altering the thickness of the deposited film by varying dipping cycles. In this study, we report using the SILAR method[26] to deposited BiOI nanoflake arrays directly on a flexible FTO glass substrate pre-coated with a TiO_2 block layer. This initial work demonstrated a best photo-electric conversion efficiency of only 0.092%. However, this is a critical step towards environmentally friendly manufacturing in aqueous-based solution processing.[27]

The basic design principle of solar cells is to increase the optical absorption of the active layer and/or reduce the electron loss during transport. The construction of heterostructures has the potential to enhance the overall energy conversion efficiency of photovoltaic devices through the improvement of the charge separation efficiency.[28, 29] In order to achieve excellent photoelectric conversion

performance, the BiOI/Bi_2S_3 heterojunction is formed *in situ* in the visible and near IR part absorption of the solar spectrum of Bi_2S_3.[30] Meanwhile, the flexible ITO/PET substrate is utilized for large area, roll to roll manufacturing of thin-film solar cells in this work. The heterojunction films were synthesized completely in aqueous solution and the whole manufacturing process was carried out at a low temperature. To our knowledge, flexible photoelectrochemical solar cells based on BiOI/Bi_2S_3 heterojunctions are scarcely studied.

2. Experimental

2.1 Chemicals

Bismuth nitrate pentahydrate (Bi $(NO_3)_3{\cdot}5H_2O$), potassium iodide (KI), sodium sulfide nonahydrate ($Na_2S{\cdot}9H_2O$) and thioacetamide (TAA, CH_3CSNH_2) were obtained from Sinopharm Chemical Reagent Co., Ltd (China). ITO/PET flexible substrate was purchased from Nippon Sheet Glass Co., Ltd. Deionized (DI) water was used in all the experiments.

2.2 Preparation of the BiOI/Bi_2S_3 heterojunction films

BiOI nanoflake films were deposited directly on ITO/PET substrates utilizing a modified SILAR method.[26] Precursor solution containing bismuth and iodine were prepared by dissolving Bi $(NO_3)_3{\cdot}5H_2O$ and KI in DI water. KI dissolved spontaneously while Bi $(NO_3)_3{\cdot}5H_2O$ required ultrasonic assistance. To synthesize BiOI/Bi_2S_3 heterojunction films, the above prepared BiOI films were put into TAA solution for differing times (0.5, 1, 2 and 3 h) at 45 ^oC. Pure Bi_2S_3 films were also fabricated for comparison by modified SILAR method with Bi $(NO_3)_3{\cdot}5H_2O$ and $Na_2S{\cdot}9H_2O$ aqueous solution as the reactants. ITO/PET substrate was successively immersed, for 15 s each into 6 mM $Na_2S{\cdot}9H_2O$ and 4 mM Bi $(NO_3)_3{\cdot}5H_2O$ solution. Following each immersion, the substrate was rinsed for 15 s with DI water. All obtained films were air dried at 60 ^oC.

The photovoltaic cells were assembled using the prepared BiOI, Bi_2S_3 and BiOI/Bi_2S_3 heterojunction film electrodes as the working electrodes and sputtering Pt/ITO/PET as the counter electrodes. A redox (I^-/I_3^-) electrolyte composed of 0.05 M I_2, 0.5 M LiI, 0.3 M DMPII, and 0.5 M 4-TBP in 3-methoxy acrylonitrile was injected into the cell when measuring the I-V characteristics and the IPCE properties.

2.3 Characterization

The resulting thin films were characterized by X-ray diffraction (XRD, Bruker D8 Advance diffractometer) with nickel-filtered CuKα radiation: λ = 1.5418 Å and work power: 40 kV – 40 mA. SEM images were captured by field-emission scanning electron microscope (FESEM, JEOL 6700-F). The sample for high-resolution transmission electron microscopy (HRTEM) was scraped from the film on ITO/PET substrate, dispensed into ethanol using an ultrasonication process, and dropped into carbon-copper grids. TEM images were obtained using a JEOL JSM-2010FEF field emission electron microscope at an accelerating voltage of 200 kV. UV-Vis absorption spectra were recorded with UV-2550 (SHMADZU). The constituents of films were determined by Raman spectra using a Renishaw inVia Raman Microscope Raman system with laser excitation of 532 nm. X-ray photoelectron spectra (XPS) were recorded on an ESCALAB 250Xi X-ray photoelectron spectrometer using non-monochromatized Mg Kα X-ray as the excitation source and C1s as the reference line.

2.4 Photovoltaic performance measurement

Current-voltage curves were conducted using a Keithley digital source meter (Keithley 2400) by applying independently external voltage to the cell and measuring the photo-generated current out from the cell under illumination of AM 1.5 G solar simulator (Oriel, 100 $mWcm^{-2}$). The photoelectric performances fill factor (*FF*) and photo-to-electric energy conversion efficiency (η) of the flexible solar cells were calculated according to the following equations:[31]

$$FF = \frac{V_{max} \times J_{max}}{V_{oc} \times J_{sc}} \quad (1)$$

$$\eta\,(\%) = \frac{V_{max} \times J_{max}}{P_{in}} \times 100\% = \frac{V_{oc} \times J_{sc} \times FF}{P_{in}} \times 100\% \quad (2)$$

Where J_{sc} is the short-circuit current density ($mA{\cdot}cm^{-2}$), V_{oc} is the open-circuit voltage (V), P_{in} is the incident light power, J_{max} ($mA{\cdot}cm^{-2}$) and V_{max} (V) are the current density and voltage at the point of maximum power output in the *J-V* curves. The incident photon-to-current conversion efficiency (IPCE) was recorded using a power meter (Newport 69911) with irradiation by a 300 W xenon light source (Oriel) and an Oriel Cornerstone 130 1/8 m monochromator in DC mode. A reference scan with the Si detector was taken prior to the sample measurement to allow for background subtraction.

The surface photovoltage spectra (SPS) measurement system was composed of a monochromatic light, a lock-in amplifier (SR830-DSP) with a light chopper (SR540), a sample cell and a computer. A 500 W xenon lamp (CHF-XM-500W) and a double-prism monochromator provided monochromatic light. In the photovoltaic cell, ITO/PET substrates with BiOI, BiOI/Bi_2S_3 or Bi_2S_3 films acted as the bottom electrodes. A glass substrate covered with FTO was used for the top electrode and a spacer of mica was inserted between the two electrodes.

3. Results and discussion

3.1 Structural and morphological characterization

The phase and crystal structure of BiOI, Bi_2S_3 and BiOI/Bi_2S_3 hybrid films obtained under various conditions were characterized using X-ray diffraction (XRD) (Fig. 1). In all spectra, the diffraction peaks located approximately at 27, 47, and 54^o, as labeled by asterisks, are come from the ITO/PET substrate. In order to achieve a better visual effect, upper section of the peaks located at about 27^o resulting from the substrate was severed. Fig. 1a illustrates that pure BiOI is crystalline and all peaks (except for the peaks from substrate) can be readily indexed to the tetragonal phase of BiOI (JCPDS card no. 73-2062) and no other impurity peaks are observed. After the BiOI films were immersed into 5 mM TAA aqueous solution for 0.5 h, 1 h, 2 h, and 3 h, the BiOI/Bi_2S_3 hybrid structures formed, therefore we named these products BiOI/Bi_2S_3-τ (τ represents the reaction time, 0.5, 1, 2, and 3 h, respectively). The increased reaction time

gradually weakened the diffraction peaks of BiOI (Fig. 1b to 1e), demonstrating the gradually consumption of BiOI. Additional features of Bi_2S_3 are not observed in the X-ray diffraction analysis. Even the reference pure Bi_2S_3 sample showed no diffraction peaks, resulting from the amorphous nature of low temperature synthesized Bi_2S_3.

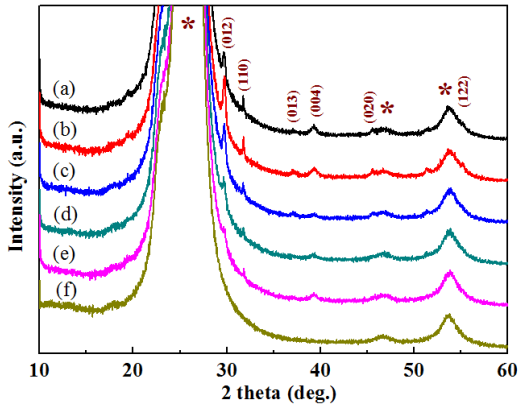

Fig. 1 XRD patterns of (a) BiOI, (b) BiOI/Bi_2S_3-0.5, (c) BiOI/Bi_2S_3-1, (d) BiOI/Bi_2S_3-2, (e) BiOI/Bi_2S_3-3 and (f) Bi_2S_3 on ITO/PET substrates. The numbers after Bi_2S_3 represent immersion time (h) of BiOI in 5 mM thioacetamide aqueous solution at 45 °C.

The morphology of the synthesized BiOI, Bi_2S_3 and BiOI/Bi_2S_3 hybrid films were further examined by field emission scanning electron microscopy (FESEM). Fig. 2a shows the typical morphology of the as-prepared BiOI films, which were fully and uniformly covered with the hierarchically crossed nanoflowers on the substrate. Individual BiOI nanoflake possesses a thickness of approximately 50 nm and a diameter of about 1 μm. Varying the cycle number (reaction time) enables the variation of both thickness and diameter of the nanoflakes. The nanoflake intersected each other and formed a compact film. Fig. 2b-2e shows the surface images of the pure BiOI and BiOI/Bi_2S_3-0.5~3.0 hybrid films.

Interestingly, the forming process of BiOI/Bi_2S_3 can be visualized and deduced through the SEM images. Fig. 2b shows that the newly formed Bi_2S_3 nanospheres are distributed sparsely on the framework of BiOI nanoflake with approximate diameter of 20 nm, when the reaction time was 0.5 h. However, we hypothesize that many tiny amorphous Bi_2S_3 nanoparticles are uniformly covering the BiOI nanoflake since the transformation of BiOI to Bi_2S_3 is a homogeneous reaction. The resulting tiny heterojunctions may provide the needed effective forces to separate photogenerated carriers. Fig. 2c-e clearly shows that the Bi_2S_3 nanospheres became larger and denser with increasing exposure in the TAA aqueous solution. The ordered 2D nanostructual BiOI nanoflake arrays were decorated with different sizes of Bi_2S_3 nanospheres to form heterojunctions. However, the BiOI nanoflake arrays are partially damaged and the thickness decreases when the reaction time was extended to 2 h (Fig. 2d), due to the etching process in the TAA solution. Further reaction will cause severe damage of the BiOI nanoflake arrays, as shown in Fig. 2e. The transformation of BiOI to Bi_2S_3 results from the lower solubility ($K_{sp} = 1.0 \times 10^{-97}$) of Bi_2S_3 in aqueous solution compared to BiOI ($K_{sp} = 1.8 \times 10^{-31}$) and is accomplished by an anion exchange reaction[32-36]. The BiOI remained in the film even after a 48 h reaction, which is probably due to the compact coverage of Bi_2S_3 on the BiOI exterior. The morphology of pure Bi_2S_3 obtained by a same low temperature and selected SILAR method is depicted in Fig. 2f. SEM observation reveals that such a Bi_2S_3 film consists of nano-sized particles. The amorphous sample was further annealed at 250 °C for 30 min for crystallization and XRD characterization. The corresponding diffraction peaks are indexed to the standard PDF card of orthorhombic structure Bi_2S_3 (JCPDS card no.17-320), as shown in Fig. S1.

More detailed microscopic characterizations of the BiOI/Bi_2S_3 heterostructure were determined using transmission electron microscopy (TEM), high-resolution TEM (HRTEM), and selected area electron diffraction (SAED). The TEM image of BiOI/Bi_2S_3-1 heterostructure is shown in Fig. 3a. The Bi_2S_3 nanosphere is converted from BiOI and tightly attached on BiOI. Fig. 3b and c show the HRTEM images of BiOI and Bi_2S_3 from the heterostructure. The adjacent lattice spacing of *ca.* 0.277 nm (Fig. 3b) is in agreement with the (001) plane of tetragonal BiOI. Corresponding SAED pattern of BiOI (Fig. 3d) exhibits strong ordered electron-diffraction spots, demonstrating that BiOI is a single crystal with high crystallinity. However, Bi_2S_3 emerged as an amorphous phase due to the lack of lattice fringe in the HRTEM of Bi_2S_3 (Fig. 3c), electron-diffraction spots, or rings in the SAED pattern (not shown).

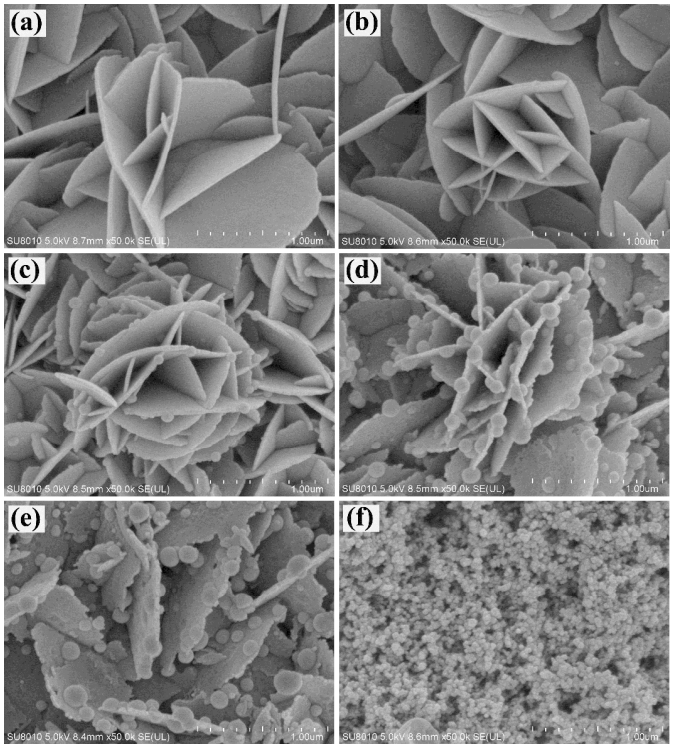

Fig. 2 FESEM images of (a) BiOI, (b) BiOI/Bi_2S_3-0.5, (c) BiOI/Bi_2S_3-1, (d) BiOI/Bi_2S_3-2, (e) BiOI/Bi_2S_3-3 and (f) pure Bi_2S_3 on ITO/PET substrates.

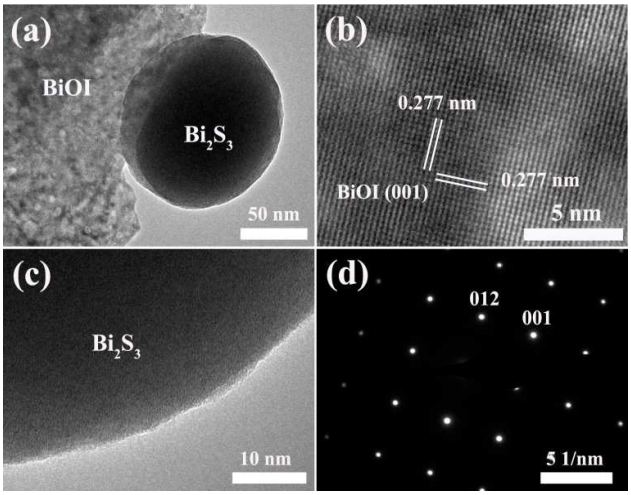

Fig. 3 (a) TEM image of BiOI/Bi_2S_3-1 heterojunction, HRTEM images of BiOI (b) and Bi_2S_3 (c) from the heterojunction, (d) selected-area electron diffraction pattern of BiOI in (a).

3.2 Optical characterization

Raman spectroscopy is an effective tool to characterize the composition of films. To further investigate the structural information of BiOI, BiOI/Bi_2S_3 and Bi_2S_3 films, we recorded the Raman spectra between 50 and 400 cm^{-1} at room temperature. These spectra were collected *in situ* on the ITO/PET substrate (Fig. 4). The pure BiOI film exhibits two distinct absorptions at 84.5 cm^{-1} and 149.6 cm^{-1}, respectively (Fig. 4a). The 149.6 cm^{-1} band is assigned to the E_g internal Bi-X stretching mode.[9, 35, 37] After heterojunction formation with Bi_2S_3, the peak intensity of BiOI distinctly decreased, which can be attributed to the transformation of BiOI to Bi_2S_3. Meanwhile, a novel peak near 99.4 cm^{-1} emerged, which is assigned to the A_g phonon mode of Bi_2S_3.[38] Raman spectra of BiOI/Bi_2S_3-3 and pure Bi_2S_3 are shown in Fig. S2. The absorptions at 237.3 cm^{-1} and 260.2 cm^{-1} of heterostructures agree well with previous reports[39, 40] and results from the anti-symmetric stretching vibration of Bi-S in Bi_2S_3.[41]

XPS was employed to further evaluate the composition of the optimized BiOI/Bi_2S_3-0.5 since the Bi_2S_3 signal in this sample could not be detected by Raman spectroscopy. The XPS spectra reveal that the film is composed of Bi, I, O, S, and C (Fig. S3a). The two strong peaks at 159.1 and 164.4 eV in the high-resolution XPS spectra (Fig. S3b) are assigned to Bi $4f_{7/2}$ and Bi $4f_{5/2}$, respectively. The peak at 225.7 eV corresponds to the S 2s transition (Fig. S3c). Thus, we believed that BiOI/Bi_2S_3 heterojunctions have been successfully obtained using this novel solution process.

The absorbency of photoanode material can influence the photoelectric conversion of solar cells significantly. Therefore, the optical properties of the synthesized films were also characterized by ultraviolet (UV)-vis absorption spectroscopy. Fig. 5a shows the UV-vis absorption spectrum of the synthesized BiOI nanoflake film, which has an optical absorption edge of 650 nm. The corresponding band gap value is roughly calculated using: E_g (eV) = 1240/absorption edge (nm), resulting in a band gap of 1.90 eV. This is in good agreement with reported values in the literature.[10, 19, 42, 43] The absorbance was enhanced at the short wavelength range (400-550 nm) for the BiOI/Bi_2S_3 film, and the absorption range was gradually extended to near-infrared region when more Bi_2S_3 formed (Fig. 5b-5e). In particular, a noticeable shoulder peak was observed around 700 nm in the spectrum of BiOI/Bi_2S_3-3, while the absorption edge range of BiOI/Bi_2S_3-0.5 and BiOI/Bi_2S_3-1.0 was not obvious. The improvement of optical properties is attributed to the addition of Bi_2S_3, which possesses higher absorption efficiency and a narrower band gap. For the pure Bi_2S_3 film (Fig. 5f), its absorption curve is very similar with the BiOI/Bi_2S_3-3 sample, indicating that most of the BiOI has been transformed into Bi_2S_3 in the BiOI/Bi_2S_3-3 sample.

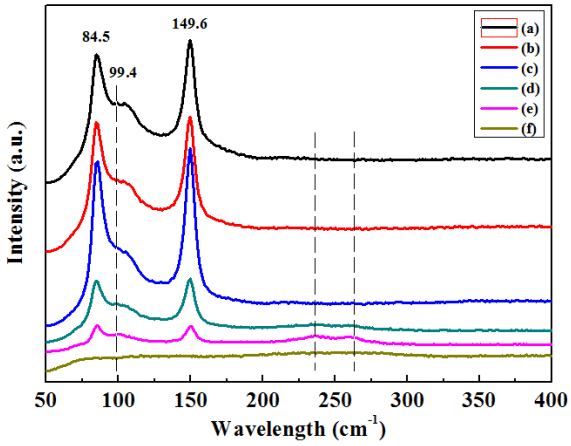

Fig. 4 Raman spectra of (a) BiOI, (b) BiOI/Bi_2S_3-0.5, (c) BiOI/Bi_2S_3-1, (d) BiOI/Bi_2S_3-2, (e) BiOI/Bi_2S_3-3 and (f) Bi_2S_3 on ITO/PET substrates.

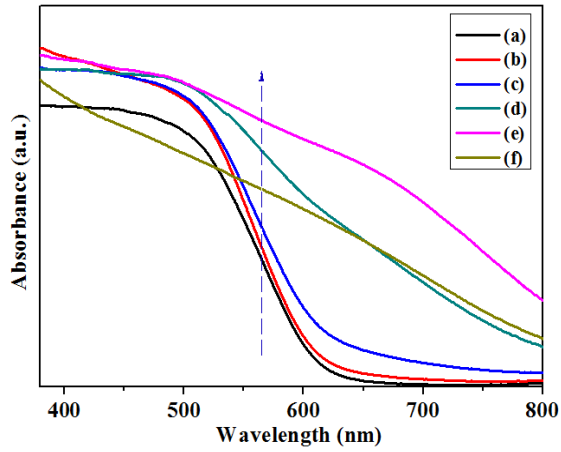

Fig. 5 Optical absorption spectra of BiOI nanoflake arrays (a), Bi_2S_3 nanosphere particles (f) and BiOI/Bi_2S_3 heterostructures (b-e) on ITO/PET substrates. The arrow in the figure is a guide for absorbance increase of different samples.

3.3 Photovoltaic performance

Similar to the case of Dye Sensitized Solar Cells (DSSCs), the operating principle of our device is divided into three parts. First, the incident photons are absorbed by BiOI/Bi_2S_3 active layer and the charge carriers are generated (both of them possess suitable band

gaps to absorb a wide range of the simulated solar spectrum). Next, the electrons excited from Bi_2S_3 are injected into BiOI and transferred to the ITO substrate together with electrons excited from BiOI. Meanwhile, the holes from BiOI and Bi_2S_3 are captured by I^- in the electrolyte and diffuse to the Pt counter electrode. Finally, the oxidized I_3^- is reduced by an e^- from external circuit.

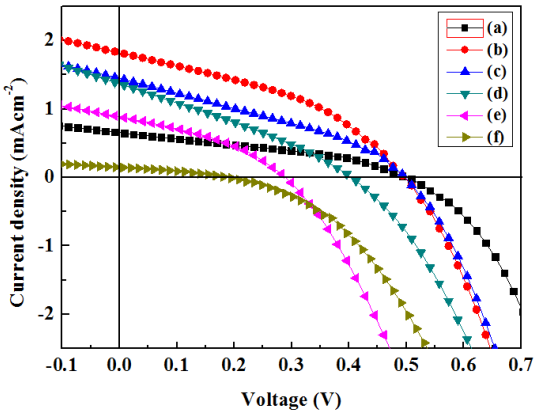

Fig. 6 Typical I-V characteristics of (a) BiOI, (b) BiOI/Bi_2S_3-0.5, (c) BiOI/Bi_2S_3-1, (d) BiOI/Bi_2S_3-2, (e) BiOI/Bi_2S_3-3 and (f) Bi_2S_3 based flexible solar cells measured under simulated one-sun AM 1.5G illumination.

Table 1 Summary of device performance for various PV devices based on BiOI/Bi_2S_3

Device no.	V_{oc} (V)	J_{sc} (mA cm^{-2})	*FF* (%)	η (%)
(a)	0.50	0.65	36.5	0.12
(b)	0.50	1.82	40.0	0.36
(c)	0.50	1.45	33.4	0.24
(d)	0.40	1.37	29.7	0.16
(e)	0.29	0.89	36.7	0.09
(f)	0.19	0.15	33.4	0.009

Measurements were performed under AM 1.5G one sun (light intensity: 100 mW cm^{-2}), the active areas were ca. 0.20 cm^2 for all of the cells.

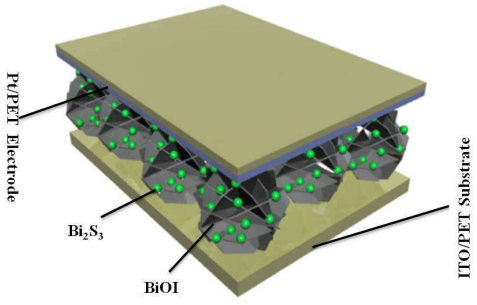

Scheme 1 the schematic structure of photoelectrochemical solar cells based on BiOI/Bi_2S_3 heterojunctions.

To evaluate the electron transport property and light harvesting efficiency, the synthesized BiOI, Bi_2S_3 and BiOI/Bi_2S_3 hybrid films were fabricated into photoanodes and the photovoltaic properties of these photoelectrochemical cells were analyzed by the current density-voltage (*J-V*) curves (Fig. 6). Fig. 6a shows the typical current density-voltage (*J-V*) characteristic of the pure BiOI-based flexible solar cell obtained with I^-/I_3^- liquid electrolyte under simulated AM 1.5G illumination. Detailed photovoltaic performance parameters are listed in Table 1. The short-circuit photocurrent density (J_{sc}), open-circuit voltage (V_{oc}), fill factor (*FF*), and power conversion efficiency (η) are 0.65 mAcm^{-2}, 0.50 V, 0.365, and 0.12%, respectively for the pure BiOI based cell, consistent with the flexible BiOI solar cell as previously reported.[44] In the case of BiOI/Bi_2S_3-0.5 (Fig. 6b), the photovoltaic performance is significantly improved due to the increase of J_{sc} (almost three times greater than pure BiOI based cell), and partly by the improvement of FF. Nevertheless, the V_{oc} of BiOI/Bi_2S_3-0.5 is unchanged. As the immersion time of BiOI in TAA aqueous solution was prolonged, the photovoltaic performance diminished gradually (Fig. 6c-d). Not until the immersion time of 3 h (Fig. 6e) does the device performance begins to be inferior to the primary pure BiOI-based one. The pure Bi_2S_3-based solar cell was also fabricated for comparison, which exhibits negligible photoelectric response compared to the best BiOI/Bi_2S_3-0.5 device showed above (Fig. 6b). This unsatisfactory performance is attributed to the poor crystallinity of the Bi_2S_3 film, which likely leads to a high rate of recombination centers and low carrier mobilities.[30] The schematic structure of photoelectrochemical solar cells based on BiOI/Bi_2S_3 heterojunctions was shown in scheme 1.

The dark current arises from the reduction of I_3^- ion by the electrons from the ITO substrate and BiOI nanoflake surface. This causes electron recombination resulting in a decrease in photocurrent, preventing the recapture of injected electrons by I_3^- at the photoanode is critical to reduce the current leakage in DSSC.[45,46] Fig. S4 shows the dark current density-voltage characteristics of BiOI and BiOI/Bi_2S_3 heterojunction based devices with the applied bias from 0 to +0.75 V. The onsets of the dark current of BiOI, BiOI/Bi_2S_3-0.5 and BiOI/Bi_2S_3-1 based devices occurred at abias about 0.45 eV, which is in accordance with the V_{oc} of these three devices, determined by the Fermi level of the BiOI and the redox potential of I^-/I_3^- electrolyte.[47-49] However, the onsets for BiOI/Bi_2S_3-2 and BiOI/Bi_2S_3-3 shifted to a lower forward bias, indicating a higher recombination rate between the transferred electrons and I_3^- ions, which is mainly due to the damage of BiOI structures in the BiOI/Bi_2S_3-2 and BiOI/Bi_2S_3-3 films as shown in the SEM images (Fig. 2d-e), meaning that the electron transportation was impeded and directly resulted in the inferior V_{oc}[50] in such samples.

The incident photo-to-current conversion efficiency (IPCE) spectra of various photoanodes were utilized to provide further evidence of the improvement in J_{sc} of the Bi_2S_3 decorated BiOI nanoflake arrays. The IPCE is defined as the ratio of the number of electrons in the external circuit produced by an incident photo at a given wavelength divided by the number of incident photons.[51] To simplify the analysis process, IPCE spectra of three representative samples were chosen. Fig. 7 shows the IPCE spectra of BiOI, BiOI/Bi_2S_3-0.5 and BiOI/Bi_2S_3-3 based solar cells as a function of the illumination wavelength, which is in agreement with photoelectric conversion efficiency of the solar cells (Fig. 6 and Table 1). The IPCE spectra exhibit a sharp cutoff in the ultraviolet less than 400 nm, which is due to optical absorption by PET. The maximum value of the IPCE of BiOI/Bi_2S_3-0.5 based solar cell is approximately 47.8%, higher than both BiOI (31.1%) and BiOI/Bi_2S_3-3 (41.5%) based solar cells. Interestingly, BiOI/Bi_2S_3-0.5 based solar cells have no photoresponse beyond 650 nm, while the

BiOI/Bi_2S_3-3 one has photoresponse up to 800 nm, which is consistent with the optical absorption spectra (Fig. 5). The IPCE is rationalized using the following equation:[52]

$$IPCE(\lambda) = LHE\ \eta_{separate}(\lambda)\ \eta_{transport}(\lambda)$$

where LHE is the light-harvesting efficiency, related to the optical absorption spectra, $\eta_{separate}$ is the electron-hole separate efficiency, and $\eta_{transport}$ is the charge transport efficiency. The IPCE augment of BiOI/Bi_2S_3-0.5 is partially deciphered from the UV-vis absorption spectrum (Fig. 5b), as discussed above. However, the limited increase of photo absorption is not significant enough to explain the three times higher saturation photocurrent density value.[53] Another impact factor to the IPCE is the charge transport efficiency. Both electron and hole transports are critical and affected by bulk and surface recombination processes. These processes can be qualitatively explained by the dark current-voltage characteristics, since BiOI and BiOI/Bi_2S_3-0.5 based solar cells showed no significant charge transport efficiency difference due to highly similar dark current onsets. The third factor affecting the IPCE value is the charge separate efficiency.

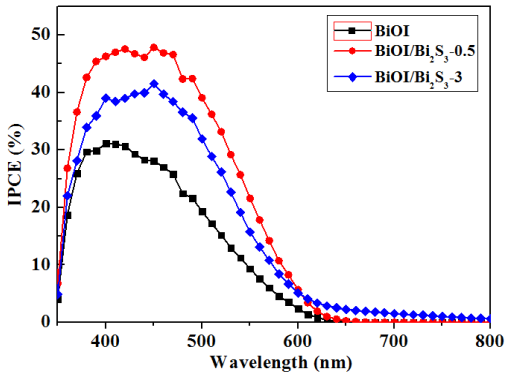

Fig. 7 Incident photo-to-current conversion efficiency (IPCE) spectra of BiOI, BiOI/Bi_2S_3-0.5 and BiOI/Bi_2S_3-3 based solar cells as a function of the illumination wavelength.

In pH 7.0, the corresponding E_{VB} and E_{CB} of Bi_2S_3 were 1.05 and −0.33 eV while those of BiOI were 1.91 and 0.15 eV (versus NHE), respectively. To investigate the charge separation and transfer behavior at the surface/interface as well as the optical characteristics of BiOI and BiOI/Bi_2S_3 heterojunction films under illumination, the surface photovoltage spectra (SPS) experiments were conducted. Fig. 8 shows the SPS spectra of pure BiOI and BiOI/Bi_2S_3 heterojunction films (the monochromatic light is irradiated from the surface of the samples), and the corresponding SPV phase spectra were shown in Fig. S5. After the semiconductor receives photons of appropriate energy, the absorbed photons induce the formation of free charge carriers by creating electron–hole pairs via band-to-band transitions in the vicinity of the surface. For p-type semiconductor, the photoinduced electron accumulates at the surface while for n-type semiconductor the holes move to the surface. The SPV phase value of p-type semiconductor is 90~180° or -90~-180° and the n-type semiconductor is 0~90° or 0~-90°. Our experimental results (Fig. S5a and S5e) followed the above conclusions. The SPV response range of pure BiOI film was about 350-600 nm, which is in accordance with the optical absorption data (Fig. 5a). More interestingly, the minimum value of the SPV emerged at 520 nm and the corresponding SPV phase value shift about 180°C (Fig. S5a), indicating that the transport directions of photoinduced charges via band-to-band transitions are opposite to the direction of charges diffuse from the surface to the bulk or from the bulk to the surface after 520nm. However, the SPV value of BiOI/Bi_2S_3-0.5 heterojunction film has no decrease at 520 nm (Fig. 8b), which is the effect of interfacial electric field in BiOI/Bi_2S_3-0.5 heterostructure film. The SPV response with visible light irradiation is the effect of surface electric field and interface electric field simultaneously.[54] As we know that the SPV signal is proportional to the amount of charges Q and the charge separation distance d ($SPV \approx Qd$), excitons generated in BiOI and Bi_2S_3 contribute to the SPV signal and result in a larger total charge Q, implying random exciton diffusion toward the interface. and then separation the charge carriers diffuse away from the interface, enhancing the charge separation distance d.[55] Base on the above discussion, we can conclude that the photoinduced charges could be efficiently separated at the interface of BiOI/Bi_2S_3-0.5 heterojunction. Moveover, the photoresponse of heterostructure semiconductors at short wavelength is consistent with the photoresponse of the outer semiconductor in heterostructure. The minimum SPV value shifts from 520 nm to 470 nm with the increase of Bi_2S_3 and the SPV response of BiOI/Bi_2S_3-2 heterostructure film starts to weaken before 520 nm when the immersion time of BiOI nanoflake in TAA solution is greater than 2 hours (Fig. 8d). This is likely caused by the severe destruction of the framework of the BiOI nanoflake due to the transformation of BiOI to Bi_2S_3 and Bi_2S_3 nanoparticles aggregation on the surface of BiOI nanosheets. Additionally, the photoelectrochemical cells based on BiOI/Bi_2S_3-2 and BiOI/Bi_2S_3-3 hybrid films possessed a stronger and wider light absorption but drastically decreased J_{sc}, V_{oc} and η compared to BiOI/Bi_2S_3-0.5. This is likely due to the reduced efficiency of separation and transfer of charge carriers at interface of BiOI/Bi_2S_3 heterojunction.

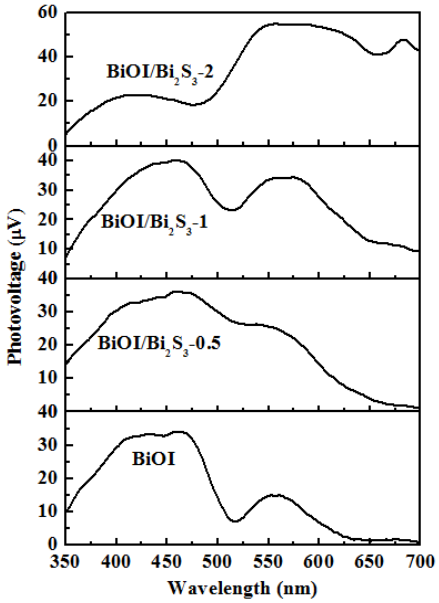

Fig. 8 The SPS responses of pure BiOI and BiOI/Bi_2S_3 heterostructure films.

Considering all the three factors, light absorption, charge separation and transport properties, the most pronounced effect for IPCE and photovoltaic properties improvement of BiOI/Bi_2S_3 based solar cell is the efficient charge separation in the interface of the BiOI/Bi_2S_3 heterojunctions and a minor effect in the improvement of light absorption. Thus, an appropriate transformation degree of BiOI to Bi_2S_3 is essential to facilitate charge separation and light harvesting to eventually improve the overall conversion efficiency of the photoelectrochemical cell.

4. Conclusions

In summary, a new type of flexible heterojunction photoanode architecture was created by *in situ* decorating BiOI nanoflake array films with Bi_2S_3 nanospheres through a simple solution process at a relative low temperature. We have discovered and carefully investigated the photoelectrochemical properties of these BiOI/Bi_2S_3 heterojunction films for use in solar cells. Owing to the increase of photo absorption and more efficient charge separation efficiency, while retaining the similar charge transport efficiency, a short-circuit current density of 1.82 $mAcm^{-2}$ and photo-to-electricity conversion efficiency of 0.36% was achieved by partially decorating the BiOI nanoflake array film with a little bit of Bi_2S_3 nanospheres (BiOI/Bi_2S_3-0.5) as photoanode, which is nearly three times higher than the bare BiOI nanoflake array based cell. Along with more Bi_2S_3 particles formed, the perfect BiOI nanoflake framework was gradually broke down and resulted in lower conversion efficiency, which demonstrates that an appropriate transformation degree of BiOI to Bi_2S_3 is critical to improve the photoelectrochemical cell efficiency. Significant improvement for V_{oc} and FF of these solar cells will likely be achieved once an ideal blocking layer under BiOI is applied, or crystalline Bi_2S_3 are used. This new photoelectrochemical cell design is appealing for low-cost, large-area, roll-to-roll application as in the manufacturing of third generation thin-film photovoltaics.

Acknowledgements

This work was supported by the National Natural Science Foundation of China (21273192, 61204009). Innovation Scientists and Technicians Troop Construction Projects of Henan Province (Grant No. 144200510014) and Program for Innovative Research Team (in Science and Technology) in University of Henan Province (Grant No.2012IRTSTHN021).

Notes and references

[a] *Key Laboratory of Micro-Nano Materials for Energy Storage and Conversion of Henan Province and Institute of Surface Micro and Nano Materials, Xuchang University, Henan 461000, P.R. China. E-mail: zzheng@xcu.edu.cn; Fax: +86-374-296-8988; Tel: +86-374-296-8988.*

[b] *Key Laboratory of Pesticide & Chemical Biology of Ministry of Education, College of Chemistry, Central China Normal University, Wuhan 430079, P.R. China. E-mail: zhanglz@mail.ccnu.edu.cn, Fax: +86-27-6786-7535; Tel: +86-27-6786-7535.*

† Footnotes should appear here. These might include comments relevant to but not central to the matter under discussion, limited experimental and spectral data, and crystallographic data.

Electronic Supplementary Information (ESI) available: XRD pattern of Bi_2S_3 on ITO glass, Raman spectra of BiOI/Bi_2S_3-3 and pure Bi_2S_3, XPS analysis of BiOI/Bi_2S_3-0.5, J-V characteristics in the dark, and phase spectra. See DOI: 10.1039/b000000x/

1 G.-V. Irene and L.-C Monica, *Energ Environ. Sci.*, 2009, **2**, 19-34.
2 A. Hagfeldt, G. Boschloo, L. Sun, L. Kloo and H. Pettersson, *Chem. Rev.*, 2010, **110**, 6595-6663.
3 A. Yella, H.-W. Lee, H. N. Tsao, C. Yi, A. K. Chandiran, M. K. Nazeeruddin, E. W.-G Diau, C.-Y. Yeh, S. M. Zakeeruddin and M. Grätzel, *Science*, 2011, **334**, 629-634.
4 B. O'Regan and M. Grätzel, *Nature*, 1991, **353**, 737-740.
5 S. K. Poznyak and A. I. Kulak, *Electrochim. Acta*, 1990, **35**, 1941-1947.
6 H. Z. An, Y. Du, T. M. Wang, C. Wang, W. C. Hao and J. Y. Zhang, *Rare Metals*, 2008, **27**, 243-250.
7 Y. Lei, G. Wang, S. Song, W. Fan, M. Pang, J. Tang and H. Zhang, *Dalton Trans.*, 2010, **39**, 3273-3278.
8 R. Bonnaire, *C. R. Acad. Sci., Paris*, 1968, **266**, 1415-1418.
9 J. E. D. DAVIES, *J. Inorg. Nucl. Chem.*, 1973, **35**, 1531-1534.
10 M. V. Shtilikha and D. V. Chepur, *Sov. Phys. Semicond.*, 1972, **6**, 962-964.
11 M. V. Shtilikha and V. Y. Slivka, *Inorg. Mater.*, 1975, **11**, 319-320.
12 J. Bordas, J. Robertson and A. Jakobsson, *J. Phys. C: Solid State Phys.*, 1978, **11**, 2607-2621.
13 Y. Y. Li, J. S. Wang, H. C. Yao, L. Y. Dang and Z. J. Li, *J. Mol. Cata. A: Chem.*, 2011, **334**, 116-122.
14 J. X. Xia, S. Yin, H. M. Li, H. Xu, L. Xu and Q. Zhang, *Colloid Surf. A*, 2011, **387**, 23-28.
15 Y. N. Wang, K. J. Deng and L. Z. Zhang, *J. Phys. Chem. C*, 2011, **115**, 14300-14308.
16 L. Q. Ye, L. H. Tian, T. Y. Peng and L. Zan, *J. Mater. Chem.*, 2011, **21**, 12479-12484.
17 S. X. Ge, K. Zhao and L. Z. Zhang, *J. Nanopart. Res.*, 2012, **14**, 1015-1026.
18 J. X. Xia, S. Yin, H. M. Li, H. Xu, Y. S. Yan and Q. Zhang, *Langmuir*, 2011, **27**, 1200-1206.
19 X. Xiao and W.-D. Zhang, *J. Mater. Chem.*, 2010, **20**, 5866-5870.
20 X. Zhang, L. Z. Zhang, T. F. Xie and D. J. Wang, *J. Phys. Chem. C*, 2009, **113**, 7371-7378.
21 H. F. Cheng, B. B. Huang, Y. Dai, X. Y. Qin and X. Y. Zhang, *Langmuir*, 2010, **26**, 6618-6624.
22 G. P. Dai, J. G. Yu and G. Liu, *J. Phys. Chem. C*, 2011, **115**, 7339-7346.
23 J. Jiang, X. Zhang, P. Sun and L. Z. Zhang, *J. Phys. Chem. C*, 2011, **115**, 20555-20564.
24 K. Zhao, X. Zhang and L. Z. Zhang, *Electrochem. Commun.*, 2009, **11**, 612-615.
25 Y. F. Nicolau, *Appl. Surf. Sci.*, 1985, **22/23**, 1061-1074.
26 K. W. Wang, F. L. Jia, Z. Zheng and L. Z. Zhang, *Electrochem. Commun.*, 2010, **12**, 1764-1767.
27 L. Martinez, M. Bernechea, F. P. G. de Arquer and G. Konstantatos, *Adv. Energy. Mater.*, 2011, **1**, 1029-1035.
28 T. Arai, M. Yanagida, Y. Konishi, Y. Iwasaki, H. Sugihara and K. Sayama, *J. Phys. Chem. C*, 2007, **111**, 7574-7577.
29 M. Law, L. E. Greene, A. Radenovic, T. Kuykendall, J. Liphardt and P. D. Yang, *J. Phys. Chem. B*, 2006, **110**, 22652-22663.
30 G. Konstantatos, L. Levina, J. Tang and E. H. Sargent, *Nano Lett.*, 2008, **8**, 4002-4006.
31 M. Grätzel, *Prog. Photovolt: Res. Appl.*, 2000, **8**, 171-185.

32 J. Cao, B. Y. Xu, H. L. Lin, B. D. Luo and S. F. Chen, *Catal. Commun.*, 2012, **26**, 204-208.
33 H. F. Cheng, B. B. Huang, X. Y. Qin, X. Y. Zhang and Y. Dai, *Chem. Commun.*, 2012, **48**, 97-99.
34 D.-K. Ma, M.-L. Guan, S.-S. Liu, Y.-Q. Zhang, C.-W. Zhang, Y.-X. He and S.-M. Huang, *Dalton Trans.*, 2012, **41**, 5581-5586.
35 J. Cao, B. Y. Xu, H. L. Lin, B. D. Luo and S. F. Chen, *Dalton Trans.*, 2012, **41**, 11482-11490.
36 Z. Liu, J. Z. Fang, W. C. Xu, X. X. Xu, S. X. Wu and X. M. Zhu, *Mater. Lett.*, 2012, **88**, 82-85.
37 F. Dong, Y. J. Sun, M. Fu, Z. B. Wu and S. C. Lee, *J. Hazard. Mater.*, 2012, **219-220**, 26-34.
38 Y. Y. Zhao, K. T. E. Chua, C. K. Gan, J. Zhang, B. Peng, Z. P. Peng and Q. H. Xiong, *Phys. Rev. B*, 2011, **84**, 205330.
39 X.-H. Liao, H. Wang, J.-J. Zhu and H.-Y. Chen, *Mater. Res. Bull.*, 2001, **36**, 2339-2346.
40 Y. W. Koh, C. S. Lai, A. Y. Du, E. R. T. Tiekink and K. P. Loh, *Chem. Mater.*, 2003, **15**, 4544-4554.
41 T. Lutz, A. MacLachlan, A. Sudlow, J. Nelson, M. S. Hill, K. C. Molloy and S. A. Haque, *Phys. Chem. Chem. Phys.*, 2012, **14**, 16192-16196.
42 J. Henle, P. Simon, A. Frenzel, S. Scholz and S. Kaskel, *Chem. Mater.*, 2007, **19**, 366-373.
43 X. Zhang and L. Z. Zhang, *J. Phys. Chem. C*, 2010, **114**, 18198-18206.
44 K. W. Wang, F. L. Jia and L. Z. Zhang, *Mater. Lett.*, 2013, **92**, 354-357.
45 S. Ito, P. Liska, P. Comte, R. Charvet, P. Pechy, U. Bach, L. Schmidt-Mende, S. M. Zakeeruddin, A. Kay, M. K. Nazeeruddin and M. Grätzel, *Chem. Commun.*, 2005, 4351-4353.
46 A. Zaban, A. Meier and B. A. Gregg, *J. Phys. Chem. B*, 1997, **101**, 7985-7990.
47 T. W. Hamann and J. W. Ondersma, *Energ Environ. Sci.*, 2011, **4**, 370-381.
48 B. E. Hardin, H. J. Snaith and M. D. McGehee, *Nat. Photonics*, 2012, **6**, 162-169.
49 A. J. Nozik, *Philos. Trans. R. Soc. A*, 1980, **295**, 453-470.
50 B. Tan and Y. Y. Wu, *J. Phys. Chem. B*, 2006, **110**, 15932-15938.
51 J. R. Mann, M. K. Gannon, T. C. Fitzgibbons, M. R. Detty and D. F. Watson, *J. Phys. Chem. C*, 2008, **112**, 13057-13061.
52 I. Bedja, P. V. Kamat, X. Hua, A. G. Lappin and S. Hotchandani, *Langmuir*, 1997, **13**, 2398-2403.
53 I. S. Cho, C. H. Lee, Y. Z. Feng, M. Logar, P. M. Rao, L. L. Cai, D. R. Kim, R. Sinclair and X. L. Zheng, *Nat. Commun.*, 2013, **4**, 1723.
54 T. F. Jiang, T. F. Xie, Y. Zhang, L. P. Chen, L. L. Peng, H. Y. Li and D. J. Wang, *Phys. Chem. Chem. Phys.*, 2010, **12**, 15476-15481.
55 D. Gross, I. Mora-Sero, T. Dittrich, A. Belaidi, C. Mauser, A. J. Houtepen, E. Da Como, A. L. Rogach and J. Feldmann, *J. Am. Chem. Soc.*, 2010, **132**, 5981-5983.